

# Microseismic Precursory Characteristics of Rock Burst Hazard in Mining Areas Near a Large Residual Coal Pillar: A Case Study from Xuzhuang Coal Mine, Xuzhou, China

An-ye Cao<sup>1,2</sup> · Lin-ming Dou<sup>1,2</sup> · Chang-bin Wang<sup>1,2</sup> · Xiao-xiao Yao<sup>1,2</sup> · Jing-yuan Dong<sup>3</sup> · Yu Gu<sup>3</sup>

Received: 8 October 2015 / Accepted: 21 June 2016 / Published online: 1 July 2016  
© Springer-Verlag Wien 2016

**Abstract** Identification of precursory characteristics is a key issue for rock burst prevention. The aim of this research is to provide a reference for assessing rock burst risk and determining potential rock burst risk areas in coal mining. In this work, the microseismic multidimensional information for the identification of rock bursts and spatial–temporal pre-warning was investigated in a specific coalface which suffered high rock burst risk in a mining area near a large residual coal pillar. Firstly, microseismicity evolution prior to a disastrous rock burst was qualitatively analysed, and the abnormal clustering of seismic sources, abnormal variations in daily total energy release, and event counts can be regarded as precursors to rock burst. Secondly, passive tomographic imaging has been used to locate high seismic activity zones and assess rock burst hazard when the coalface passes through residual pillar areas. The results show that high-velocity or velocity anomaly regions correlated well with strong seismic activities in future mining periods and that passive tomography has the potential to describe, both quantitatively and periodically, hazardous regions and assess rock burst risk. Finally, the bursting strain energy

index was further used for short-term spatial–temporal pre-warning of rock bursts. The temporal sequence curve and spatial contour nephograms indicate that the status of the danger and the specific hazardous zones, and levels of rock burst risk can be quantitatively and rapidly analysed in short time and in space. The multidimensional precursory characteristic identification of rock bursts, including qualitative analysis, intermediate and short-time quantitative predictions, can guide the choice of measures implemented to control rock bursts in the field, and provides a new approach to monitor and forecast rock bursts in space and time.

**Keywords** Rock burst · Microseismic precursory characteristics · Passive velocity tomography · Bursting strain energy index · Spatial–temporal pre-warning

## 1 Introduction

Rock bursts, a type of dynamic geological hazard in underground coal mining, are characterised by sudden release of strain energy accumulated in a coal and rock mass. They can result in serious damage to underground workings or surface buildings, and in some cases, injury and loss of life (Gibowicz and Kijko 1994; Dou et al. 2012). The dynamic hazards are encountered in many coal mines due to large-scale rupture or movement of hard strata, irregular layout of the coalface, large mining depth, reaction of anomalous geological structures, etc., and become progressively more severe as the average depth and extent of mining operations increase (Cao 2009; Li et al. 2007). For example, on 30 July 2010, a rock burst occurred during the dip entry excavation at a mining depth of over 1050 m in Zhangshuanglou Coal Mine, a 200-m-long dip entry was damaged, and six workers were killed. On 11 August 2010,

✉ Chang-bin Wang  
cumtwangchangbin@163.com

An-ye Cao  
caoanye@163.com

<sup>1</sup> Key Laboratory of Deep Coal Resource Mining, Ministry of Education of China, School of Mines, China University of Mining and Technology, Xuzhou 221116, Jiangsu, China

<sup>2</sup> State Key Laboratory of Coal Resource and Mine Safety, China University of Mining and Technology, Xuzhou 221116, Jiangsu, China

<sup>3</sup> Xuzhuang Coal Mine, Datun Energy Company Limited, Xuzhou 221600, Jiangsu, China

a rock burst of magnitude 2.7 occurred in the LW25110 headentry of Yuejin Coal Mine, and a 340-m-long entry ahead of the face was severely damaged (Lu et al. 2015). On 3 November 2011, a rock burst accident of magnitude 4.1 induced by a large thrust fault caused 10 deaths and trapped 75 people during the headentry excavation of LW21221 in Qianqiu Coal Mine (Cai et al. 2014). On 15 March 2013, a rock burst disaster happened in Junde Coal Mine due to the periodic caving of a hard gritstone stratum. In the accident, 21 workers were trapped, and five killed (Lu et al. 2015). On 27 March 2014, another severe rock burst was triggered by the fracturing of super-thick conglomerate stratum in LW21032, Qianqiu Coal Mine, and six workers were killed. The aforementioned accidents attracted the attention of the Chinese Government and society at large. Investigations conducted by State Administration of Coalmine Safety (China) shows that the number of coal mines in China which experienced rock burst hazards has increased from 32 in 1985 to 142 in 2012 (Pan et al. 2013). In China, the occurrence of rock bursts has been one of the most serious, and least understood, problems in deep coal mining.

Several methods to assess rock burst risks and determine potential rock burst areas have been reported, such as microseismic monitoring (Jiang et al. 2006; Lu et al. 2010; Xia et al. 2010; Cao et al. 2012; Konicek et al. 2013; Feng et al. 2015), electromagnetic emission (He et al. 2011a; Wang et al. 2011), acoustic emission (He et al. 2011b), drilling bits (Dou and He 2001; Gu et al. 2012), pressure sensor installation (Zhang et al. 2014). Among them, due to the advantages of real-time monitoring, regional detection range, large size of data set, or non-destructive effects on production, etc., microseismic monitoring has been proven to be a powerful tool for quantifying seismicity and can contribute valuable information for seismic hazard evaluation (Tang et al. 2010; Xu et al. 2011).

The basic principle of microseismic monitoring involves obtaining seismic waves released by the fracturing of a coal-rock mass using seismic sensors which are spatially distributed around the targeted area, and then processing the obtained seismic waves to determine basic parameters of seismic events, e.g. source location, seismic energy, frequency, wave velocity. Based on this, one can infer the stress state, detect structural defects, and evaluate rock burst hazard (Holub et al. 2011; Dou et al. 2012; Cai et al. 2014). For instance, Brady and Leighton (1977) found that a rock burst was preceded by a rapid increase in seismic activity and was followed by a distinct decrease before the burst by a more moderate rock burst. Williams et al. (1992) investigated the fault-slip source mechanism for a rock burst that occurred at the Lucky Friday Mine. Ortlepp (2000) provided a strong evidence for extremely violent fracturing-induced significant rock bursts in the faulting process of a highly stressed remnant in a gold mine by

seismic monitoring. Yamada et al. (2007) estimated stress decreases and seismic energies of 20 events to investigate roof rupture characteristics. Chen et al. (2012) found that seismic energy and event counts steadily increased and were accompanied by a stress increase. Zhang et al. (2013) proposed a method for assessing hazards in mines based on seismic energy distribution. Zhu et al. (2015) used a computational model to estimate the abutment pressure of extremely thick alluvial strata for rock burst prevention and verified its reliability by analysing the distribution of microseismic events during mining. Besides, different seismic methods and indices for rock burst forecasting, e.g.  $b$  value,  $z$  value,  $P(b)$  value, fault total area, apparent stress, fractal dimension, were proposed by scholars at home and abroad (Xie and Pariseau 1993; Gibowicz and Kijko 1994; Fujii et al. 1997; Tang et al. 2012; Lu et al. 2015). In addition, by combining microseismic monitoring and tomographic imaging, passive velocity tomography, which relies on the transmission of seismic waves through a coal-rock mass, has become more regularly used for geological structure exploration, stress redistribution imaging, and rock burst hazard assessment (Lurka 2008; Luxbacher et al. 2008; Gong 2010; Cai et al. 2014; Cao et al. 2015; Wang et al. 2015). As a consequence of this, meaningful results have been obtained from microseismic information for better understanding the process and mechanism inducing rock bursts. Meanwhile, due to the complexity and diversity of rock burst hazards, understanding microseismic multiparameter precursors and source evolution rules is still a central problem facing those monitoring, and pre-warning, of rock bursts.

The site chosen for this study is an underground longwall face (LW7332) in Xuzhuang Coal Mine, Jiangsu Province, China, where strong tremors and rock bursts are the main safety threats during coal mining, especially when LW7332 passing through an adjacent large-sized residual coal pillar. The investigation involves specific rock burst locations, seismic intensity, and source location of related seismic events, source distribution evolution rules, multiparameter precursory characteristics, spatial-temporal pre-warning, etc. It may provide a reference for assessing rock burst risk, determining potential rock burst risk areas, and then taking relevant controlling measures to mitigate these hazards.

## 2 Microseismic Spatial–Temporal Precursory Criteria of Rock Burst

### 2.1 Passive Tomography for Periodic Spatial Assessment of Rock Burst

In coal mines, the occurrence of seismic hazards is closely related to underground in situ and mining stresses. Velocity

tomography is useful when inferring the stress state and redistribution in a coal-rock mass. Thus, high seismic activity zones and seismic hazards are assessed by tomographic imaging. The method mainly relies on the variation of seismic waves transmitted through the coal-rock mass, and the parameter is the inversion of velocity distribution with travel time. Meanwhile, velocity tomography can be classified as “active” and “passive” based on the type of source used. Passive tomography, which uses mining-induced seismic events as the sources, can estimate the relatively high stress or seismic hazard periodically during mining process, with its detection area up to about 4 km<sup>2</sup> (Lurka 2008).

Velocity tomography depends on the relationship in which the wave velocity along a seismic ray is the ray path distance divided by the time to travel between the source and receiver. Suppose the ray path of the *i*th seismic wave is *l<sub>i</sub>* and the travel time is *t<sub>i</sub>*, the time is the integral of the inverse velocity, 1/*v*(*x*, *y*, *z*), or slowness, *s*(*x*, *y*, *z*), from the seismic source to the receiver, as shown in Eqs. (1) and (2) (Gibowicz and Kijko 1994; Luxbacher et al. 2008):

$$v = \frac{l}{t} \rightarrow vt = l \tag{1}$$

$$t_i = \int_{l_i} \frac{dl}{v(x, y, z)} = \int_{l_i} s(x, y, z)dl \tag{2}$$

where *v*(*x*, *y*, *z*) is the velocity (m/s), *l* is the distance (m), *t* is the travel time (s), and *s*(*x*, *y*, *z*) represents the slowness (s/m).

The ray path *l<sub>i</sub>* is usually a curve due to the complexity of the coal-rock mass; therefore, we need to discretise the inversion area to *m* grids. So, the travel time of the *i*th ray can be presented as Eq. (3):

$$t_i = \sum_{j=1}^m d_{ij}s_j \quad (i = 1, \dots, n) \tag{3}$$

where *d<sub>ij</sub>* is the distance of the *i*th ray crossing the *j*th voxel, *n* is the total number of rays, and *m* is the number of voxels.

Arranging the time, distance, and slowness for each voxel into matrices, the velocity can be determined through inverse theory as follows (Luxbacher et al. 2008):

$$\mathbf{t} = \mathbf{d}\mathbf{s} \rightarrow \mathbf{s} = \mathbf{d}^{-1}\mathbf{t} \tag{4}$$

where **t** is the column vector of travel times (*n* × 1), **d** is the matrix of ray distances (*n* × *m*), and **s** is the column vector of slowness values (*m* × 1).

Matrix inversion methods are effective, but require considerable computational power for large data sets. The most effective way to solve the inverse problem is an iterative process. Currently, the most referenced iterative method is the simultaneous iterative reconstructive technique (SIRT) (Gilbert 1972), which has been adopted here.

During coal mining, there may be positive anomalies of P-wave velocity in high stress, or stress concentration, regions, and negative anomalies of wave velocity in pressure-relief area. A velocity anomaly is expressed by Eq. (5) (Gong 2010; Dou et al. 2014):

$$A_n = \frac{v_p - v_p^a}{v_p^a} \tag{5}$$

where *v<sub>p</sub>* is P-wave velocity at a certain point, and *v<sub>p</sub><sup>a</sup>* is the average velocity of the model.

Tables 1 and 2 list the relationship between anomaly of wave velocity and stress states, and therein, a positive anomaly represents the degree of stress concentration, whereas a negative anomaly represents the extent of fracturing and weakening of the rock mass induced by mining or artificial disturbances. This relationship can be used as the criteria for determining potential rock burst risk by passive tomography.

**Table 1** Relationship between positive anomalies of wave speed and stress concentration

Rock burst risk index	Stress concentration degree	Positive velocity anomaly <i>A<sub>n</sub></i> (%)
0	None	<5
1	Weak	5 to 15
2	Moderate	15 to 25
3	Strong	>25

**Table 2** Relationship between negative anomalies of wave speed and stress reduction

Stress reduction degree	Stress reduction characteristics	Negative velocity anomaly <i>A<sub>n</sub></i> (%)
0	None	−7.5 to 0
1	Weak	−15.0 to −7.5
2	Moderate	−25.0 to −15.0
3	Strong	<−25.0

## 2.2 Bursting Strain Energy for Short-Term Spatial–Temporal Pre-warning of Rock Burst

The preparation process of seismic hazards, e.g. earthquakes, rock bursts, is essentially the deformation, damage, and instability process of a seismic source. Seismic energy and event count are basic microseismic parameters used for field monitoring, and they have been widely used to describe the deformation and failure intensity of coal-rock mass, stress level, and seismic hazard risk in coal mining. However, they are not appropriate for quantitative analysis and assessment of seismic hazard.

Although passive tomographic imaging can quantitatively and periodically (e.g. weekly, fortnightly, or monthly) describe the hazardous region and evaluate rock burst risk during coal mining, it is still difficult to use in the short term (e.g. daily) for the spatial, or temporal, pre-warning of rock burst events. Thus, it is necessary to establish a new index that can reflect the seismicity, allied activities, and meet the requirements of quantitative, short-term, assessment of rock burst risk.

It has been shown that the elastic strain rebound increment generating an earthquake is proportional to the square root of the energy of the earthquake (Benioff 1951). To characterise in particular seismic sources, the stress release of seismic hazards seems to be more appropriate for scaling than the energy release (Kracke and Heinrich 2004). Thus, it is advantageous to choose the square root of the released energy of seismic source for seismic hazard risk assessment. As a consequence, a time-normalised index  $W_{et}$ , namely bursting strain energy, is established for temporal short-term pre-warning of rock bursts: it is developed as follows (Cai 2015a):

$$W_{et} = \frac{\varepsilon_E - \varepsilon_{E0}}{\varepsilon_{EI} - \varepsilon_{E0}}, \quad \varepsilon_E = \sqrt{\sum_{i=1}^n E_i} \tag{6}$$

where  $0 \leq W_{et} \leq 1$ , and its grade division for rock burst pre-warning is given in Table 3;  $\varepsilon_E$  is a specific strain equivalent, while its value is equal to the square root of released energy of seismic source;  $\varepsilon_{EI}$  is the critical strain equivalent, which can be obtained by sample training of occurred mine tremors in the statistical area of interest;  $\varepsilon_{E0}$  is the initial strain equivalent, and its default setting is 0;  $n$  is total seismic event count after the last macro-fracturing

event;  $E_i$  is released energy of the  $i$ th tremor after the last macro-fracture (J).

In the calculations, when  $\varepsilon_E$  reaches, or exceeds,  $\varepsilon_{EI}$ , the curve will decline to zero. Meanwhile, if the total energy released in the tremors per day has declined for three successive days (the time can be adjusted according to real conditions) and the maximum individual tremor energy per day is larger than the average energy value of background tremors, the curve will decline to a weaker level.

Meanwhile, a bursting strain energy index in the space domain  $W_{es}$ , which is defined as the sum of strain energy per unit area and unit time, is constructed for spatial short-term assessment of potential rock burst risk area, as shown in Eq. (7) (Cai et al. 2015):

$$W_{es} = \lg\left(\frac{\sum_{i=1}^n \sqrt{E_i}}{ST}\right) = \lg\left(\frac{\varepsilon_E}{ST}\right) \tag{7}$$

where  $S$  is the area of statistical zone ( $m^2$ ),  $T$  is the statistical time (days), and the duration adopted in this research is 30 days;  $E_i$  is the released energy of the  $i$ th seismic event in the statistical zone and statistical time (J).

## 3 Site Characteristics

### 3.1 Longwall Details

The selected coalface, LW7332 in Xuzhuang Coal Mine, is located in Xuzhou City, northwest of Jiangsu Province, China. Xuzhuang Coal Mine suffers high rock burst risk and is a characteristic coal mine with rock burst hazards. According to incomplete statistics, at least five disastrous rock bursts have occurred in this mine.

As shown in Fig. 1, the strike length and inclined length of LW7332 are 1200 and 205 m, respectively. The south and east sides of LW7332 border Fault F117 and the unmined coal mass, and the north side is adjacent to the goafing of LW7222 and LW7235, while the west sides border the protective pillar area of No. II3 Mining District Rise. Meanwhile, the coal pillar width between LW7332 and LW7222 goafing is 6 m, while the pillar width between LW7332 and LW7235 goafing is increased to about 22 to 25 m. According to our numerical simulation results, the stress concentration within 10- to 30-m-wide pillars is very high, while

**Table 3** Relationship between bursting strain energy index and rock burst risk

Risk index	Rock burst risk degree	Bursting strain energy index $W_{et}$ (%)
0	None	<25
1	Weak	25 to 50
2	Moderate	50 to 75
3	Strong	>75



**Fig. 1** Layout of LW7332 in the No. II3 mining district

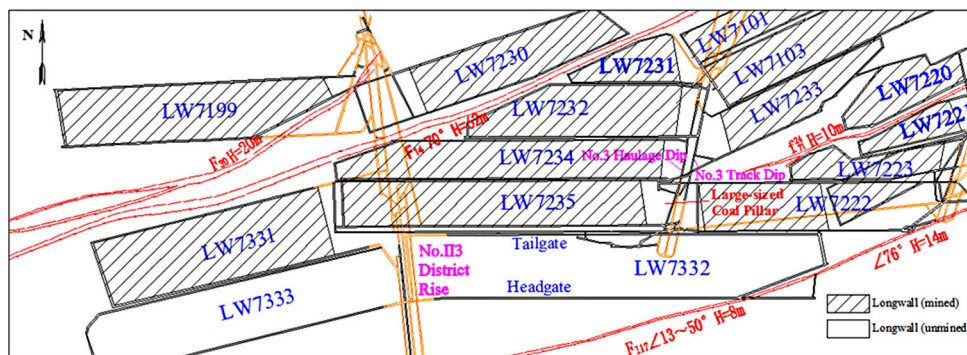
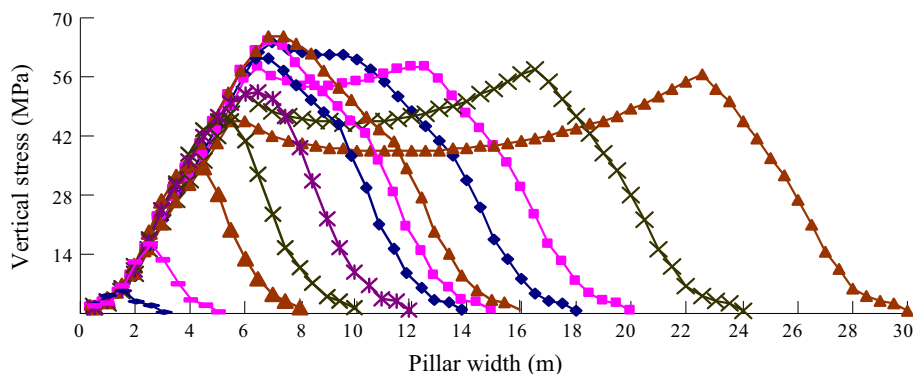


**Fig. 2** Vertical stress distribution within coal pillars with different widths



relatively small, or very large, pillars may bear a relatively lower static stress (see Fig. 2). Thus, the LW7332 tailgate near the LW7235 goafing lies in a higher static stress state during mining operations. In addition, to protect the No. 3 Track Dip and Haulage Dip which are located in the rock beds under the No. 7 Coal Seam, a large (150 m × 140 m) residual coal pillar was established between the stop lines of LW7222 and LW7235. Therefore, the width-varying section of coal pillar and adjacent large pillar may constitute a main cause of high stress concentration and high rock burst risk near the tailgate of LW7332, especially during the mining period which sees the face advancing towards, and then out of, the zone of influence of the large residual pillar.

Figure 3 shows the synthesis column map of Borehole 19 in LW7332. No. 7 Coal Seam, which is the mining coal layer of LW7332, has a cover depth varying from 551 to 668 m. The thickness of the coal seam ranges from 4.2 to 5.8 m (4.94 m on average) with an inclination ranging from 20° to 30° (24.8° on average). The coal seam is overlain successively by sandy mudstone (2.53 to 5.97 m in thickness, forming the immediate roof), fine sandstone (4.28 to 12.03 m in thickness, in the main roof), etc., and which are underlain successively by sandy mudstone (9.47 to 14.77 m), No. 8 Coal Seam (up to 3.93 m thick), etc. Meanwhile, No. 7 Coal Seam, the main roof, and floor were all classified as having a weak rock burst tendency by laboratory rock burst tendency identification.

Lithology	Column	Thickness/m
Gritstone		9.24~29.94 20.26
Sandy mudstone		14.28~21.78 17.85
Silt stone		2.49~7.31 5.32
Mudstone		8.54~14.61 9.37
No.6 coal seam		0~0.49 0.28
Sandy mudstone		4.14~6.29 4.98
Fine sandstone		4.28~12.03 7.26
Sandy mudstone		2.63~5.97 4.25
No.7 coal seam		4.20~5.80 4.94
Sandy mudstone		9.47~14.77 11.65
No.8 coal seam		0~3.93 2.00

**Fig. 3** Synthesis column: Borehole 19

### 3.2 Installed Seismic Monitoring System

Microseismic monitoring in mines allows seismic event location, calculation of seismic energy, and source mechanisms, infers the mining stress state, evaluates rock burst hazard, etc. Since 7 November 2014, a microseismic monitoring system called SOS, developed by the Central Mining Institute of Poland, was installed in Xuzhuang Coal Mine. SOS is mainly composed of a real-time monitoring recorder, analyser, sensors, digital transmission system, etc. The frequency range of each single vertical-component sensor is 1–600 Hz, the sampling rate is 500 Hz, it uses 16 bit A/D conversion, and the maximum data transmission rate is 1 MB/s. SOS can collect and filter seismic signals continuously and automatically, and accurately calculate the occurrence time, released energy, and three-dimensional coordinates of seismic events by using the Powell location algorithm. The constant velocity model was proposed for event location, which is calibrated by the arrival time residual error of a number of high-energy seismic signals. The system used 16 sensors that were distributed around Xuzhuang Coal Mine, and LW7332 was surrounded by a total of ten sensors (numbered 3 to 12). Figure 4 illustrates the longwall geometry and sensor locations.

## 4 Case Study

### 4.1 Process and Description of the Disastrous Rock Burst

Mining operations in LW7332 started on 4 June 2014, while seismic monitoring around LW7332 had been ongoing since 7 November 2014. At that period, the face was retreated by about 285 m and lay about 85 m from the large-sized residual pillar near the LW7332 tailgate. By 17 December 2014, LW7332 had retreated adjacent to the residual pillar, and 59 strong tremors with seismic energies

ranging from  $10^4$  to  $10^5$  J were recorded during this period (see Fig. 5a), mainly occurring ahead of the face and near the pillar. One hundred and eight strong tremors with a seismic energy greater than  $10^4$  J (eight tremors with energies over  $10^5$  J) occurred between 17 December 2014 and 11 March 2015 (see Fig. 5b), when the face was retreated through the residual pillar. By 13 April 2015, LW7332 had retreated about 68 m past the residual pillar, and 21 strong tremors with a seismic energy  $>10^4$  J (one tremor with an energy  $>10^5$  J) were recorded during this period (see Fig. 5c). These mainly occurred near the LW7332 tailgate and within the pillar. Many of the strong tremors induced underground strata effects to different extents.

At 6:08:33 and 6:12:48, on 14 April 2015, two strong tremors with energies of  $1.35 \times 10^4$  and  $2.39 \times 10^4$  J occurred as a consequence of mining activities. They were located near the LW7332 tailgate, about 76 and 108 m from the large coal pillar (see Fig. 5d). The tremors induced serious vibration and obvious strata effects in the tail-entry. At 19:21:48 on 14 April 2015, a disastrous rock burst occurred almost in the same place (see Fig. 5d) when LW7332 had retreated by about 71 m past the residual pillar: the calculated energy release is  $2.01 \times 10^6$  J, which was the most serious tremor since LW7332 mining began. The three-dimensional coordinates ( $x$ ,  $y$ , and  $z$ ) of the source are 4614, 1726, and  $-528$  m, respectively. According to the vertical level of the source (see Fig. 5e), it can be verified that rock burst was associated with the fracturing and caving of the main stratum overlying No. 7 Coal Seam. After the rock burst happened, 15 to 88 m ahead of the coalface in the tailgate (a total of up to 73 m) was destroyed. The maximal convergence of coal mass in the down wall of the tailgate reached 1.4 m, and the winch was pushed from the sidewall to the middle of the tailgate. Hydraulic props at several sites in the gateway were pushed over, bent, and even broken off. Many bolts and cables were pulled out, and anchor nets and lines were broken. Fortunately, none of the miners were allowed to stay within the gateways 200 m ahead of the coalface during coal cutting: the rock burst caused no injury and no loss of life. Figure 6 shows the photographs of the tailgate deformation and damage resulting from the rock burst.

Actually, the width of coal pillar between LW7332 tailgate and adjacent LW7235 goafing is 22–25 m, which can generate high stress concentrations and accumulate much elastic energy within. Meanwhile, there are multiple crossing gateways near the damaged region, and the majority of located strong tremors were clustered in the vicinity of the region, and the static stress could also be easily concentrated therein. Moreover, the large protective coal pillar of No. 3 dips, together with section coal pillar and solid-coal mass of LW7332, and could well support the

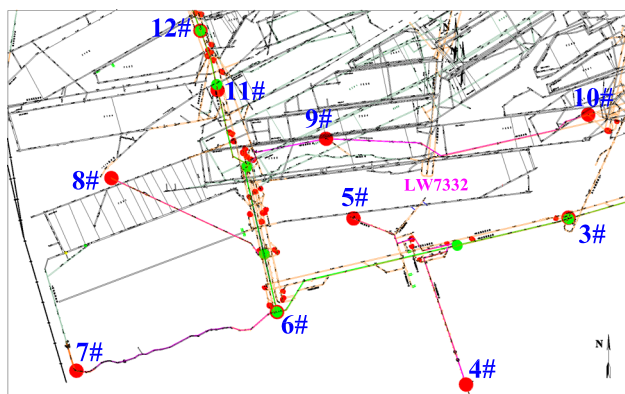
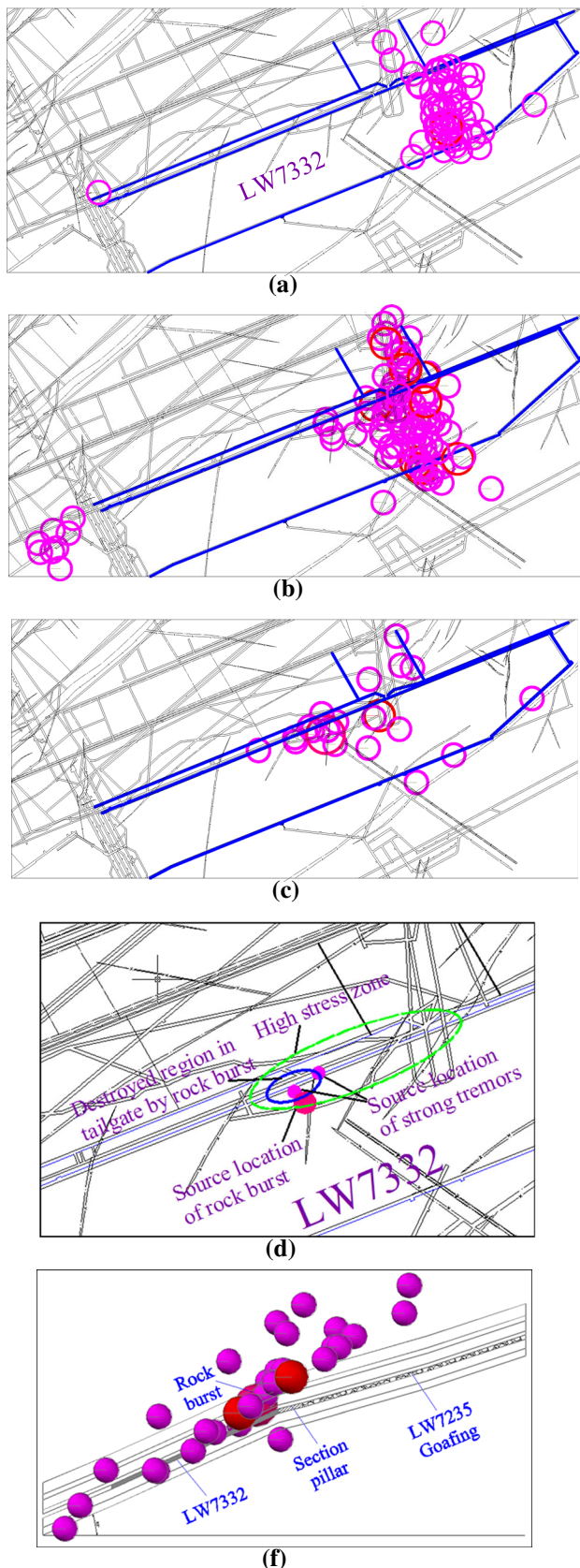


Fig. 4 Layout of sensor stations around LW7332



◀**Fig. 5** Source locations of strong tremors and rock bursts when LW7332 was retreated towards, and out of, the residual pillar zone of influence. **a** Source locations of strong tremors with energy over  $10^4$  J between 7 November 2014 and 17 December 2014. **b** Source locations of strong tremors with energy over  $10^4$  J between 18 December 2014 and 11 March 2015. **c** Source locations of strong tremors with energy over  $10^4$  J between 12 March 2015 and 13 April 2015. **d** Source locations of disastrous rock burst and two strong tremors. **e** Section view of strong tremors with energy over  $10^4$  J between 1 March 2015 and 14 April 2015, while pink points represent tremors with energies between  $10^4$  and  $10^5$  J, and red points represent tremors with energy over  $10^5$  J

overlying strata, which caused strata above LW7332 and LW7235 to be difficult to collapse regularly, and further increased the static high stress concentration in the LW7332 tailgate (see Fig. 5d); however, as LW7332 was retreated past the residual pillar, and the mined-out area increased, the bearing capacity of the coal pillar would decrease, strata overlying LW7332 and surrounding goafing areas may move together and rupture, which was considered to have been the external triggering factor for the rock burst. Ultimately, the static high stress concentration, especially when combined with the dynamic loading generated by roof caving, induced the disastrous rock burst in the LW7332 tailgate.

In summary, the rock burst was induced by the intrinsic static high stress concentration near the large residual pillar and the external strong dynamic loading generated by large-scale strata fracturing. Therefore, microseismic effects in the process of coal-rock fracturing and strata fracturing may contribute to the mechanism and early warning of rock burst.

## 4.2 Microseismic Assessment Results and Analysis

### 4.2.1 Relationship Between Microseismicity and Rock Bursting

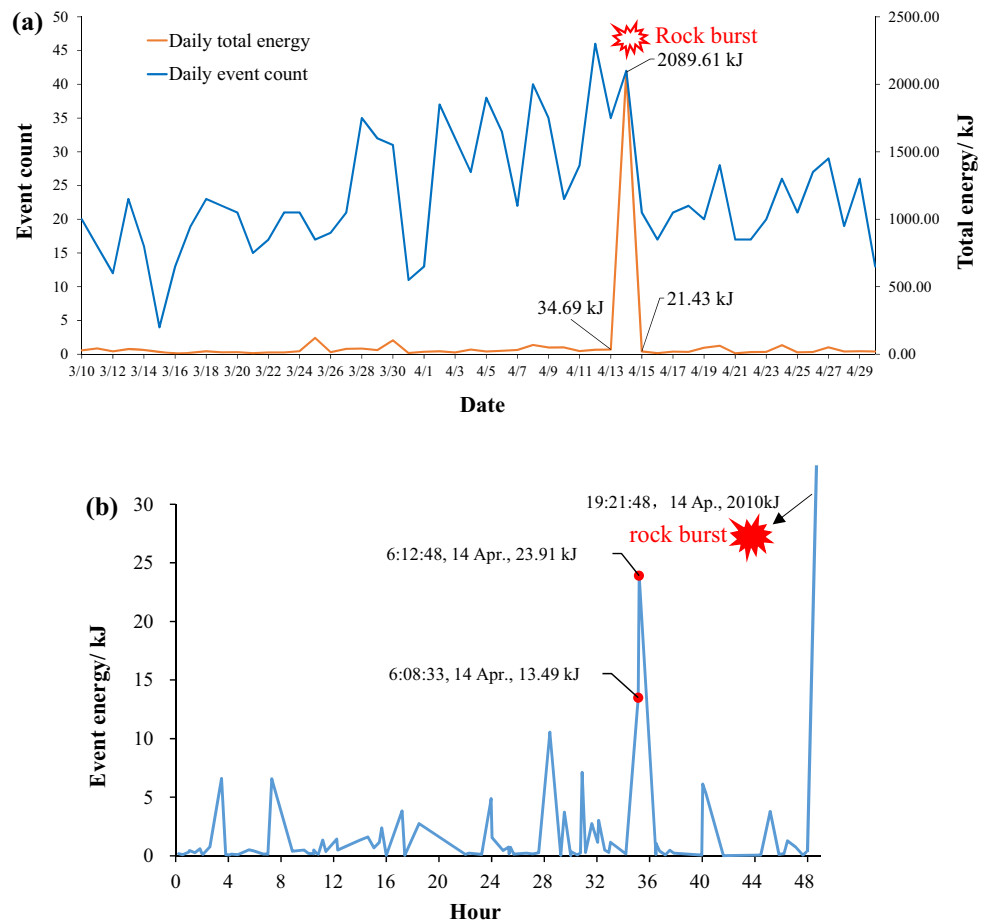
Figure 7a demonstrates the daily seismic total energy and event count variation curves from 10 March 2015 to 30 April 2015 around LW7332. Before 14 April 2015, the total energy remained stable, while the event count sharply increased, and was always maintained at high levels. Figure 7b shows the variation of seismic energy around LW7332 in the 48 h before the occurrence of a rock burst. It can be seen that two precursory strong events with energies of  $1.35 \times 10^4$  and  $2.39 \times 10^4$  J occurred consequently at 6:08:33 and 6:12:48 on 14 April 2015, which demonstrated that microfissures inside the roof stratum had propagated, converged, and connected to form a macro-fracture. The normal periodic weighting interval of the main roof was 35–63 m based on the



**Fig. 6** Rock burst damage in LW7332 tailgate on 14 April 2015



**Fig. 7** Variation of seismic energy and event count.  
**a** Variation in daily seismic total energy and event count.  
**b** Variation of seismic energy in the 48 h before the occurrence of rock burst



statistical analysis of advancing distances and pressurising processes between 4 June 2014 and 9 March 2015. However, before the rock burst, the hanging length of the main roof reached 71 m by 9 March 2015, which far exceeded the normal caving interval. Once large-scale roof fracturing and caving above LW7332 and the surrounding goafing were triggered by strong mining activity, a rock burst was inevitable. After the rock burst, both

the total seismic energy and event count suddenly decreased.

To reveal the evolutionary rule of seismic source clustering before the rock burst in the static high stress concentration zone along with LW7332 mining direction, the evolution of source distributions from 3 April to 14 April was plotted (see Fig. 8). According to Fig. 8, seismic sources began to gradually cluster and congregate at two

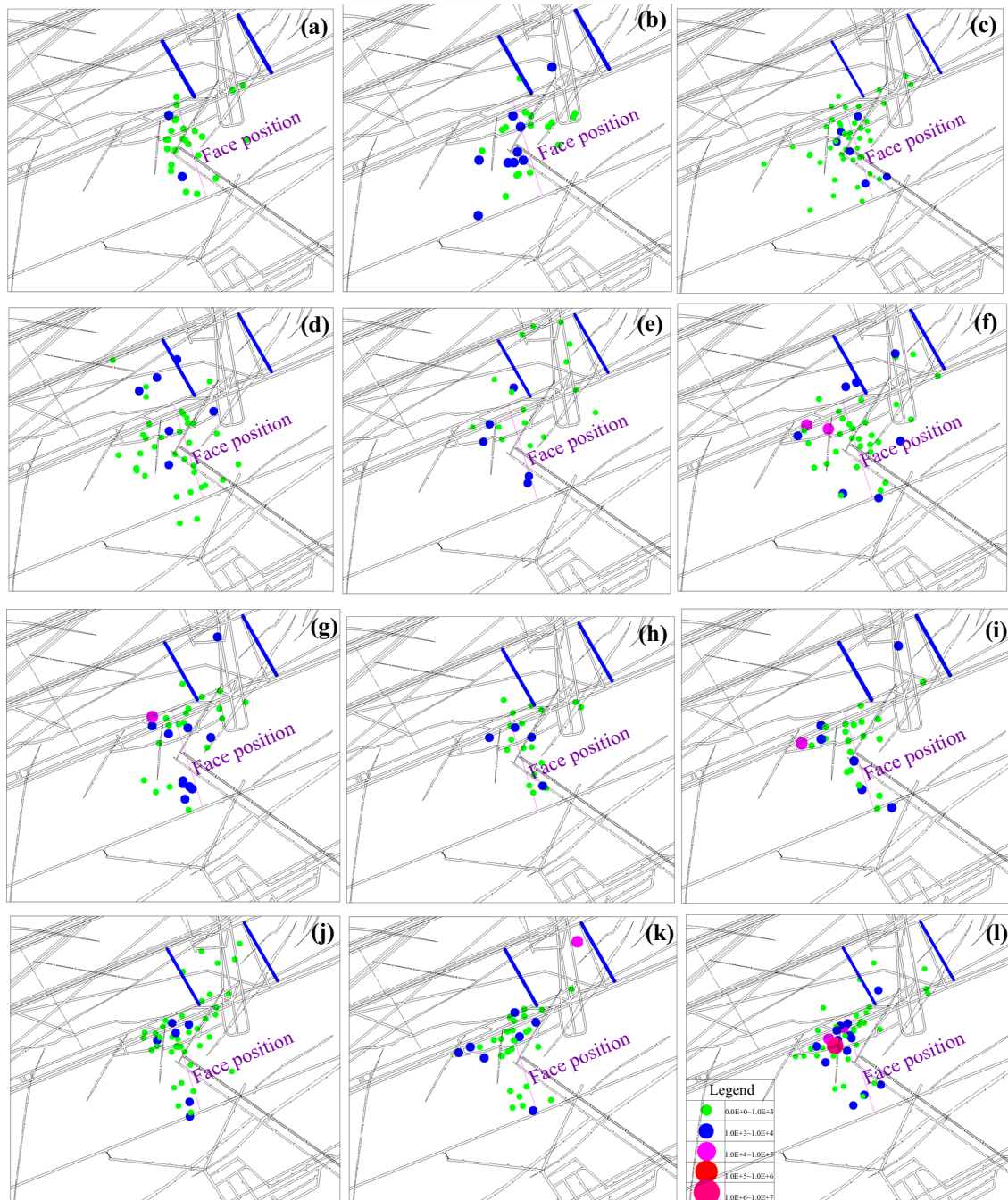


**Fig. 8** Source distribution evolution with different energy ranges from 3 April to 14 April 2015. **a** 3 April, **b** 4 April, **c** 5 April, **d** 6 April, **e** 7 April, **f** 8 April, **g** 9 April, **h** 10 April, **i** 11 April, **j** 12 April, **k** 13 April, **l** 14 April



sides of the mining position line of coalface from 3 April. The clustering was further intensified and gradually developed from two sides of the face to the tailgate side from 8 April, while high-energy events ( $E > 10^4$  J) became more frequent, which verified the propagation, convergence, and connectivity of microfissures in this coal-rock mass. Since 12 April, the sources became more significantly concentrated at the LW7332 tailgate side, which indicated that the macro-fracture in overlying strata above LW7332 and surrounding goafing had formed and that the roof structure was in a state of limit equilibrium. The rock burst was induced by the large-scale intensive dynamic loading combined with the static high stress concentration on 14 April. Thus, the abnormal clustering of seismic sources, accompanied by the high-energy-event congregation, can be regarded as a precursor to this rock burst danger.

#### 4.2.2 Passive Tomographic Results and Discussion

Passive tomographic imaging has been implemented each month for periodical spatial assessment of rock burst hazard as LW7332 passed through the large-sized residual pillar area. To improve the inversion efficiency, and avoid inconsistent spatial distributions, passive tomography was performed on LW7332 mainly using stations 3, 5, 6, 8, 9, 10, and 11, and seismic events located in the target areas. In addition, only events recorded by over five stations were selected to avoid creating artificial anomalies in the tomograms. To ensure that the ray density can satisfy the inversion requirement, and improve computational efficiency, a total of  $35 \times 35 \times 5$  voxels, with each voxel measuring  $50 \text{ m} \times 50 \text{ m} \times 175 \text{ m}$  in the X- (strike), Y- (inclination), and Z- (mining depth) directions, respectively, was input into the tomographic calculation. Inversion iteration of tomograms was conducted using SIRT

which must have an initial velocity value, and a constant P-wave velocity equal to 4300 m/s was assumed to calculate event location and perturb the first iteration. To decrease the indeterminacy, the velocity was restricted to a constant gradient of between 2.0 and 6.0 km/s. Plan views of velocity tomograms at seam level,  $Z = -560 \text{ m}$ , were generated to evaluate rock burst risk for the next mining period.

Calculated tomographic velocity images in Figs. 9, 10, 11, 12, and 13 show P-wave velocity changes during the mining period in LW7332 from 1 December 2014 and 10 April 2015. Accordingly, high-velocity and velocity anomaly regions were observed to always redistribute within the large-sized protective coal pillar and the width-varying section coal pillar ahead of the LW7332 tailgate as the face retreated passing through the residual pillar between December 2014 and February 2015. The maximum value of P-wave velocity in this period was up to 6.0 km/s, while the maximum positive velocity anomalies even exceeded 0.25, which indicates that the aforementioned areas are always at a moderate, or strong, seismic hazard risk now, and in the future. When LW7332 started to retreat past the residual pillar, the high-velocity and velocity anomaly regions were also observed to move ahead (see Fig. 12), being mainly concentrated in the tailgate side ahead of LW7332, LW7235 goafing, and part of the large-sized residual pillar. By 10 April 2015, 4 days before the rock burst, the latest velocity image was calculated based on the seismic events recorded between 21 March and 10 April. As shown in Fig. 13, high-velocity regions with higher seismic risk levels (the maximum velocity was up to 6.0 km/s, the maximum positive velocity anomalies exceeded 0.40) were observed to grow and become mainly concentrated in the tailgate side ahead, and behind, LW7332, goafings of LW7235 and 7332, etc., which indicated that there may be large-scale rupturing and

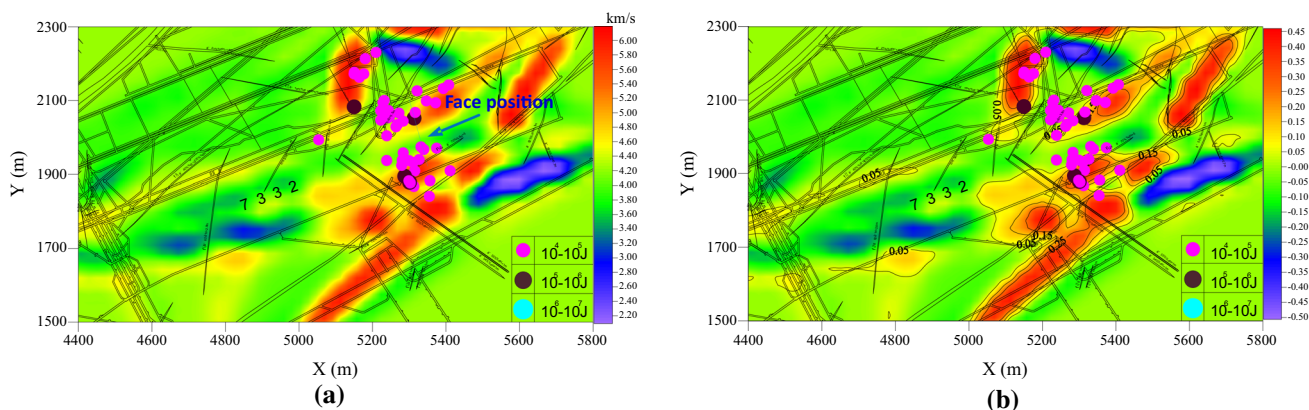


**Fig. 9** Tomographic images obtained using seismic events from 1 December to 31 December 2014 (circle symbols show positions of strong tremors with energies  $E > 10^4$  J that occurred between 1

January and 31 January 2015). **a** Velocity inversion result. **b** Velocity anomaly inversion result

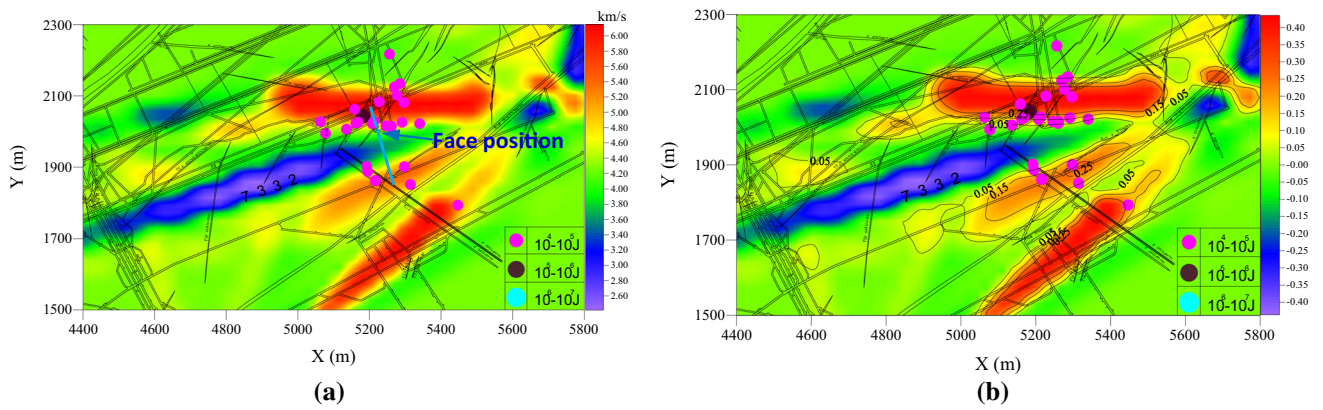


**Fig. 10** Tomographic images obtained using seismic events from 1 January to 31 January 2015 (circle symbols show positions of strong tremors with energies  $E > 10^4$  J that occurred between 1 February

and 28 February 2015). **a** Velocity inversion result. **b** Velocity anomaly inversion result

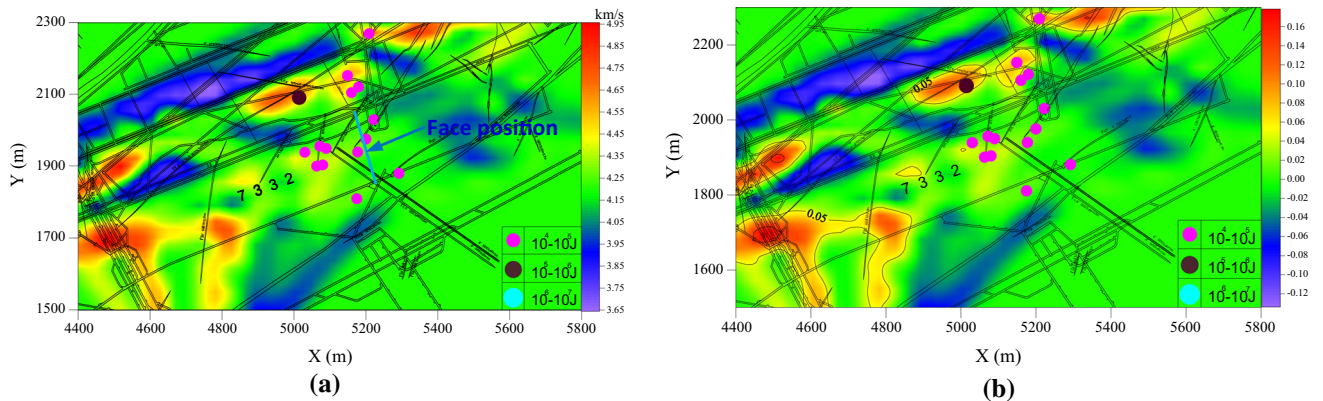


**Fig. 11** Tomographic images obtained using seismic events from 1 February to 28 February 2015 (circle symbols show positions of strong tremors with energies  $E > 10^4$  J that occurred between 1

March and 20 March 2015). **a** Velocity inversion result. **b** Velocity anomaly inversion result

movement of overlying strata above the goafing and residual pillar, causing high stress concentrations and dynamic loading near the face with the constant increase of the mined-out area.

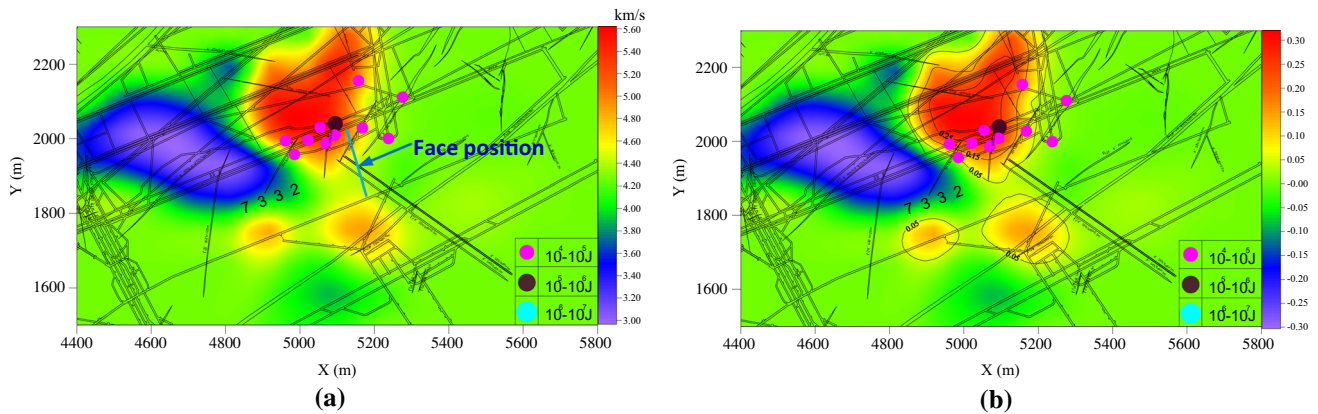
4.2.3 Bursting Strain Energy Results and Discussion

Besides periodical spatial assessment of the rock burst risk zone by passive tomographic imaging, the bursting strain energy index was further used for short-term spatial-temporal pre-warning of rock bursts during the mining of LW7332. Based on Eq. (6), the variations of bursting strain energy index from 1 January to 15 March and 15 March to 15 April 2015 were calculated as shown in Fig. 14. It is shown that the time-normalised index  $W_{et}$  of bursting strain energy accords well with the occurrence of strong tremors or strata behaviours, while  $W_{et}$  always lay at moderate or strong rock burst risk before the appearance of any tremor

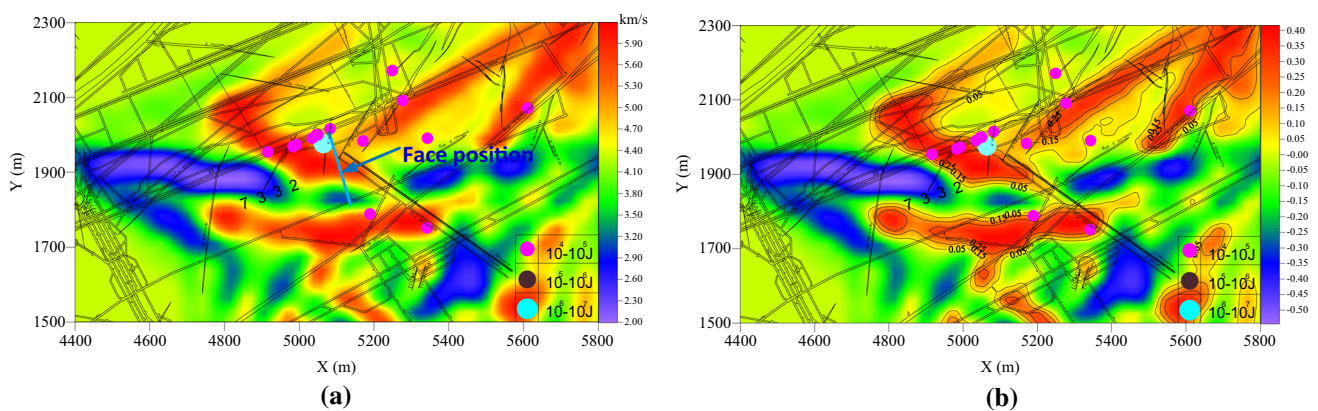
with an energy exceeding  $10^5$  J. In particular, the time-normalised index  $W_{et}$  has lain at a rock burst risk level above moderate since 6 April, then rose to over a strong risk level by 12 April, and increased constantly for 3 days until the rock burst; thereafter, the index decreased rapidly.

Figure 15 illustrates spatial contour nephograms of bursting strain energy index in space domain  $W_{es}$  during different mining periods. Nephograms show that the bursting strain energy index can effectively represent the accumulation, damage, and release processes of strain energy during the mining of LW7332, while the hypocentre of the rock burst and the destroyed zones on 14 April were nearly all located within the high seismicity and hazardous areas as pre-warned by  $W_{es}$  on 12 and 13 April 2015.

Thus, using the bursting strain energy index, the danger status, specific hazardous zones, and levels of rock burst risk can be further quantitatively analysed in short time, and in space, for the monitoring area.



**Fig. 12** Tomographic images obtained using seismic events from 1 March to 20 March 2015 (circle symbols show positions of strong tremors with energies  $E > 10^4$  J that occurred between 21 March and 10 April 2015). **a** Velocity inversion result. **b** Velocity anomaly inversion result



**Fig. 13** Tomographic images obtained using seismic events from 21 March to 10 April 2015 (circle symbols show positions of strong tremors with energies  $E > 10^4$  J that occurred between 11 April and 15 April 2015). **a** Velocity inversion result. **b** Velocity anomaly inversion result

### 4.3 Rock Burst Hazard Control

Although comprehensive pre-warning of rock bursts has been carried out in areas of LW7332 mining near a large-sized residual pillar zone, no technique was implemented to control rock burst risk before 14 April 2015. Since the disastrous rock burst happened, to reduce the static stress level and dynamic disturbance of tremors, large-diameter pressure-relief boreholes in the coal mass and directional hydraulic fracturing in the hard roof were carried out respectively in the remaining tailgate ahead of LW7332, as shown in Fig. 16.

Pressure-relief boreholes can play an important role in weakening the stress intensity in a coal mass. The specified parameters of these large-diameter boreholes in the coal mass around the LW7332 tailgate were as follows: the borehole diameter was 110 mm, the borehole depth exceeded 15 m, and the borehole interval was 2.4 m.

Directional hydraulic fracturing of the hard roof was mainly aimed at weakening the intensity of dynamic

loading induced by roof fracturing. An initial crack at the base of a borehole was formed by a special cutting tool, and the initial crack tip starts to fracture under the action of a tensile stress concentration. This crack extended rapidly along the direction of the rock level assisted by the action of high-pressure water (see Fig. 16b). The specified parameters of the hydraulic fracturing process in the main roof of the LW7332 tailgate were as follows: the height of each vertical borehole was 13 m, the borehole diameter was 42 mm, the borehole interval was 10 m, the diameter of the initial crack was 12 mm, the water injection pressure was 30 MPa, and the water flow rate exceeded 80 L/min.

By using above pressure-relief techniques, the integrity and intensity of the coal mass were destroyed and the static stress near the LW7332 tailgate was reduced, while the periodic weighting interval of the main roof was shorter, and the dynamic loading induced by strata fracturing was also weakened. Moreover, an artificial “loose and weak structure” was formed in the coal seam, which can absorb



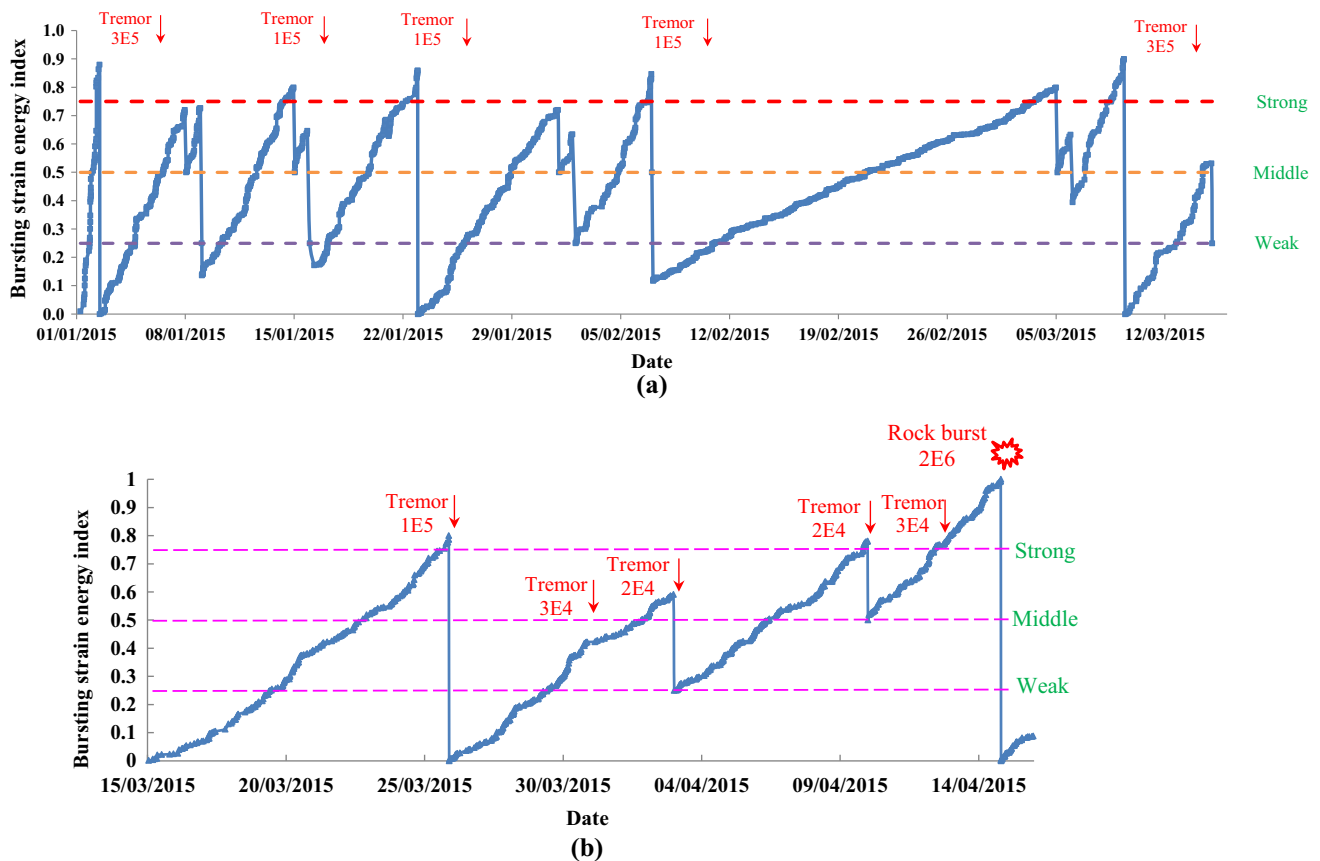


**Fig. 14** Variations of bursting strain energy index from 1 January to 15 March and 15 March to 15 April 2015. Variation of bursting strain energy index from **a** 1 January to 15 March 2015. **b** 15 March to 15 April 2015

and scatter seismic energy radiated by mining-induced tremors to a significant extent.

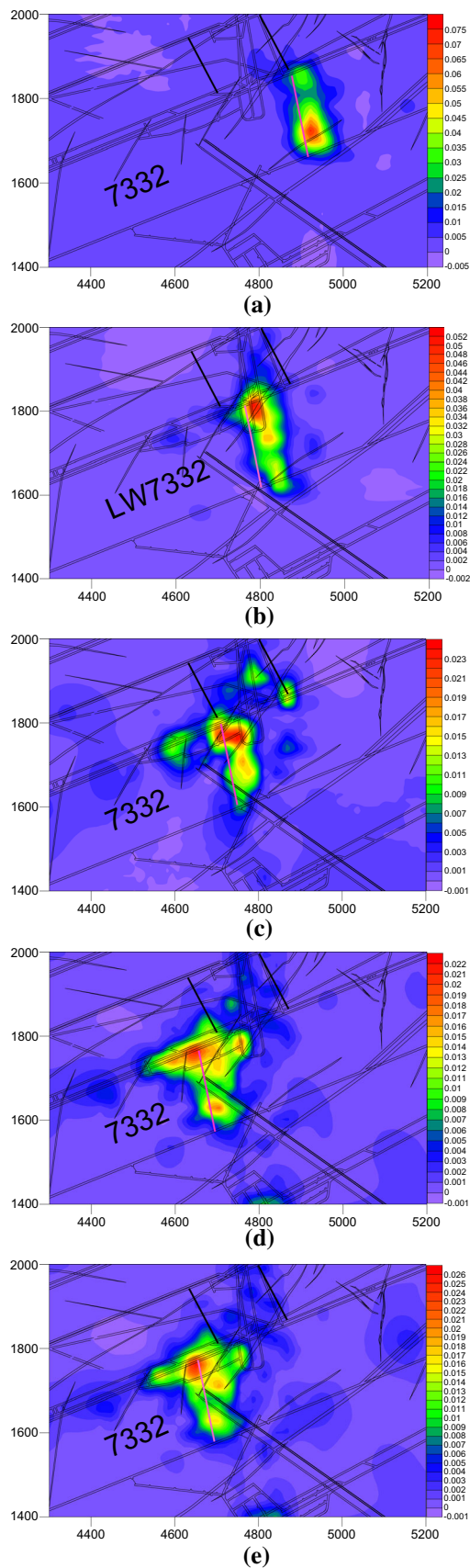
LW7332 was re-mined again from 1 May, and P-wave velocity changes during the mining period from 1 May to 30 June 2015 are shown in Figs. 17 and 18. Figure 17 indicates that the velocity near the tailgate side ahead of LW7332 decreased and the maximum positive velocity anomalies were no  $>0.05$ , while the velocity near the headgate side (ahead) was a little higher, but the maximum positive velocity anomalies were also no  $>0.20$ . The velocity and velocity anomaly shown in Fig. 18 were further reduced along with the extraction of material from the coalface, which indicated that the whole mining area of LW7332 was basically subjected to a weak seismic hazard risk. The aforementioned rock burst control techniques produced satisfactory pressure-relief results.

### 5 Conclusions

A specific coalface, LW7332 in Xuzhuang Coal Mine, which suffered from rock burst threats mainly caused by high stress concentrations from an adjacent large residual

coal pillar and width-varying section pillar, was chosen for the analysis of microseismic precursory characteristics and spatial-temporal pre-warning of rock burst hazards. The main conclusions were as follows:

1. Before the disastrous rock burst, daily seismic event count and total energy increased significantly to reflect the unstable state of energy accumulation within coal-rock mass. Daily evolution of seismic events before the rock burst indicated that rock burst was related to fracturing of roof rock layers and formation of macrofractures within the coal-rock mass. The abnormal cluster of seismic sources, abnormal variation of daily total energy and event counts, may provide a precursor to rock burst occurrence.
2. Combining seismic monitoring and tomographic imagery, passive tomographic imaging has been implemented each month for the periodic spatial assessment of rock burst hazard as LW7332 passed through the large-sized residual pillar area. The high-velocity, and velocity anomaly, regions were observed to be redistributed within the large-sized protective pillar and the width-varying section pillar ahead of the



◀**Fig. 15** Horizontal contour nephograms of  $W_{es}$  during different mining periods of LW7332. Spatial warning of  $W_{es}$  on **a** 18 September 2014, when LW7332 was mined towards a large residual pillar. **b** 15 February 2015, when LW7332 was mined ahead of half of the large residual pillar. **c** 12 March 2015, when LW7332 was just mining out past the large residual pillar. **d** 12 April 2015, 2 days before the disastrous rock burst occurred. **e** 13 April 2015, 1 day before the disastrous rock burst occurred

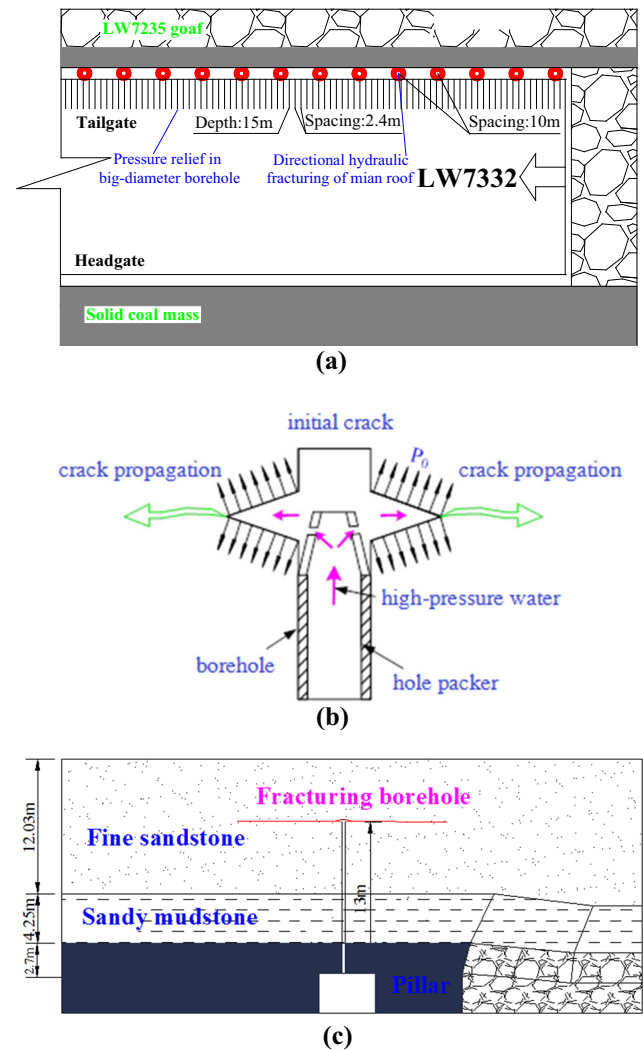


**Fig. 16** Schematic diagram of pressure relief induced by large-diameter boreholes and directional hydraulic fracturing in LW7332. **a** Plan view of the large-diameter pressure-relief boreholes and directional hydraulic fracturing boreholes in LW7332. **b** Schematic showing directional hydraulic fracturing in the roof. **c** Sectional plan through a directional hydraulic fracturing borehole in LW7332

LW7332 tailgate as the face retreated and passed through the residual pillar. Using tomographic detection practices, this technique can quantitatively and periodically describe the hazardous region and assess rock burst risks.



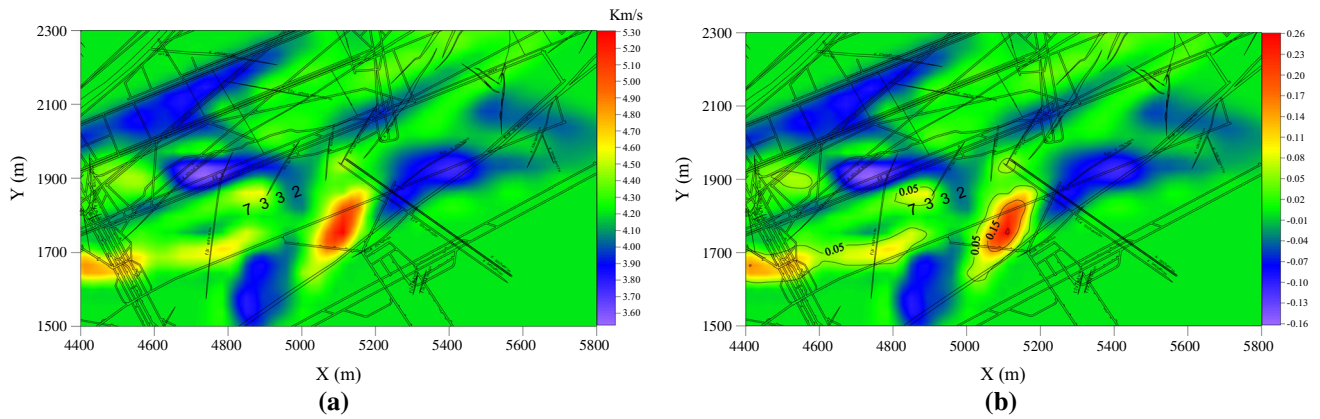


**Fig. 17** Tomographic images obtained using seismic events from 1 May to 31 May 2015. **a** Velocity inversion result. **b** Velocity anomaly inversion result

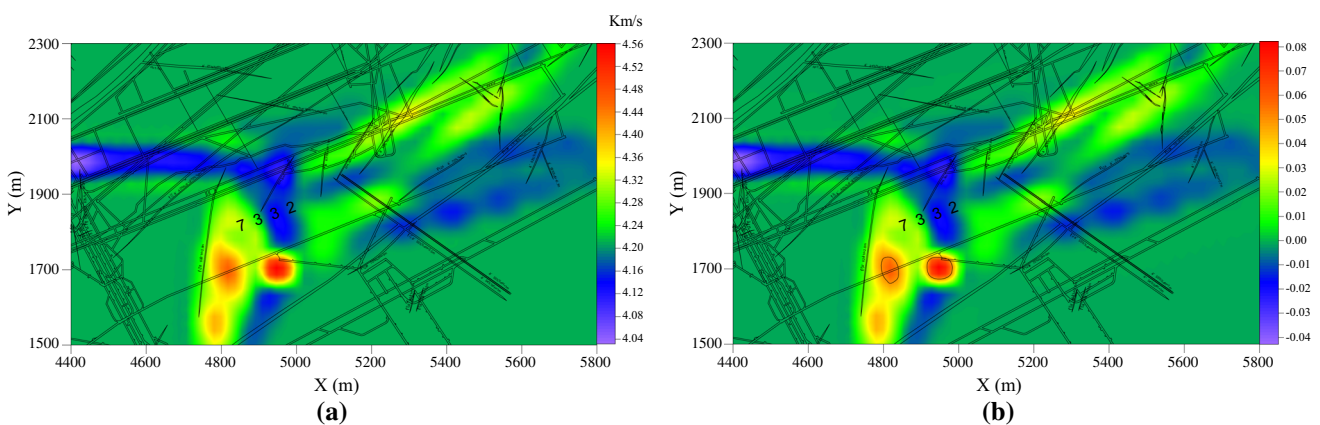


**Fig. 18** **a** Velocity inversion result. **b** Velocity anomaly inversion result

3. Bursting strain energy index was further used for short-term spatial-temporal pre-warning of rock bursts in areas of mining near the residual coal pillar. The corresponding temporal sequence curves and the horizontal contour nephograms revealed that the index can quantitatively forecast the status of the danger of a rock burst in the monitored area in short time and rapidly reflect the extent of such hazardous areas and levels of rock burst risk therein.
4. This study can improve seismic monitoring and provide a reference for rock burst pre-warning in similar coal mines. Most importantly, it should be emphasised that pre-warning of a rock burst must use the comprehensive anomaly indices including qualitative analysis of microseismicity evolution, intermediate quantitative assessment of passive velocity tomography, short-term quantitative predictions of bursting strain energy index, as well as some traditional detection methods.

**Acknowledgments** We gratefully acknowledge the financial support for this work provided by National Natural Science Foundation of China (51204165), the National Twelfth Five-year Key Science and Technology Foundation of China (2012BAK04B06), the Project of PADD funded by the Priority Academic Programme Development of Jiangsu Higher Education Instruction (SZBF2011-6-B35), and the Fundamental Research Funds for Central Universities (2014XT01, 2015XKZD04).

**References**

Benioff H (1951) Crustal strain characteristics derived from earthquake sequences. *Trans Am Geophys Union* 32:508–514

Brady BT, Leighton FW (1977) Seismicity anomaly prior to a moderate rock burst: a case study. *Int J Rock Mech Min Sci* 14:127–132

Cai W (2015a) Fault rock burst induced by static and dynamic loads superposition and its monitoring and warning. Ph.D. Thesis. China University of Mining and Technology, China (in Chinese)

Cai W, Dou LM, Cao AY, Gong SY, Li ZL (2014) Application of seismic velocity tomography in underground coal mines: a case study of Yima mining area, Henan, China. *J Appl Geophys* 109:140–149

- Cai W, Dou LM, Gong SY, Li ZL, Yuan SS (2015) Quantitative analysis of seismic velocity tomography in rock burst hazard assessment. *Nat Hazards* 75:2453–2465
- Cao AY (2009) Research on seismic effort of burst and failure of coal-rock mass associated with mining and its application. Ph.D. Thesis, China University of Mining and Technology, China (in Chinese)
- Cao AY, Dou LM, Luo X, Zhang YD, Huang JL, Andrew K (2012) Seismic effort of blasting wave transmitted in coal-rock mass associated with mining operation. *Cent South Univ Technol* 19(9):2604–2610
- Cao AY, Dou LM, Cai W, Gong SY, Liu S, Jing GC (2015) Case study of seismic hazard assessment in underground coal mining using passive tomography. *Int J Rock Mech Min Sci* 78:1–9
- Chen XH, Li WQ, Yan XY (2012) Analysis on rock burst danger when fully-mechanized caving coalface passed fault with deep mining. *Safe Sci* 50:645–648
- Dou LM, He XQ (2001) Theory and technology of rock burst prevention, China. University of Mining and Technology Press, Xuzhou, pp 82–83
- Dou LM, Chen TJ, Gong SY, He H, Zhang SB (2012) Rockburst hazard determination by using computed tomography technology in deep workplace. *Saf Sci* 50:736–740
- Dou LM, Mu ZL, Lu CP, Cao AY, Gong SY (2014) Theory and technology of mining geophysics. Science Press, Hubei, p 175
- Feng GL, Feng XT, Chen BR, Xiao YX, Yu Y (2015) A microseismic method for dynamic warning of rockburst development processes in tunnels. *Rock Mech Min Sci* 48(5):2061–2076
- Fujii Y, Ishijima Y, Deguchi G (1997) Prediction of coal face rockbursts and microseismicity in deep longwall coal mining. *Int J Rock Mech Min Sci* 34(1):85–96
- Gibowicz SJ, Kijko A (1994) An introduction to mining seismology. Academic Press, San Diego, pp 22–23
- Gilbert P (1972) Iterative methods for the three-dimensional reconstruction of an object from projections. *J Theor Biol* 36:105–117
- Gong SY (2010) Research and application of using mine tremor velocity tomography to forecast rockburst danger in coal mine. Ph.D. Thesis. China University of Mining and Technology, China (in Chinese)
- Gu S, Wang C, Jiang B, Tan Y, Li N (2012) Field test of rock burst danger based on drilling pulverized coal parameters. *Disaster Adv* 5:237–240
- He XQ, Chen WX, Nie BS, Mitri H (2011a) Electromagnetic emission theory and its application to dynamic phenomena in coal-rock. *Int J Rock Mech Min Sci* 48:1352–1358 (in Chinese)
- He H, Dou LM, Gong SY, Zhou P, Xue ZJ, He J (2011b) Study of acoustic emission monitoring technology for rockburst. *Rock Soil Mech* 32(4):1262–1268
- Holub K, Rusajova J, Holecko J (2011) Particle velocity generated by rockburst during exploitation of the longwall and its impact on the workings. *Int J Rock Mech Min Sci* 48:942–949
- Jiang FX, Yang SH, Cheng YH, Zhang XM, Mao ZY, Xu FJ (2006) A study on microseismic monitoring of rock burst in coal mine. *Chin J Geophys* 49(5):1511–1516 (in Chinese)
- Konicek P, Soucek K, Stas L, Singh R (2013) Long-hole destress blasting for rockburst control during deep underground coal mining. *Int J Rock Mech Min Sci* 61:141–153
- Kracke DW, Heinrich R (2004) Local seismic hazard assessment in areas of weak to moderate seismicity—case study from Eastern Germany. *Tectonophysics* 390:45–55
- Li T, Cai MF, Cai M (2007) A review of mining-induced seismicity in China. *Int J Rock Mech Min Sci* 44:1149–1171
- Lu CP, Dou LM, Wang YF, Zhang XM, Du TT (2010) Microseismic effect of coal materials rock burst failure induced by hard roof. *Chin J Geophys* 53(2):450–456 (in Chinese)
- Lu CP, He XQ, Liu GJ, Liu Y, Zhang N, Xue JH, Zhang L (2015) Microseismic multi-parameter characteristics of rockburst hazard induced by hard roof fall and high stress concentration. *Int J Rock Mech Min Sci* 76:18–32
- Lurka A (2008) Location of high seismic activity zones and seismic hazard assessment in Zabrze Bielszowice coal mine using passive tomography. *China Univ Min Technol* 18:177–181
- Luxbacher K, Westman E, Swanson P, Karfakis M (2008) Three-dimensional time-lapse velocity tomography of an underground longwall panel. *Int J Rock Mech Min Sci* 45(4):478–485
- Ortlepp WD (2000) Observation of mining-induced faults in an intact rock mass at depth. *Int J Rock Mech Min Sci* 37:423–436
- Pan JF, Mao DB, Lan H, Wang SW, Qi QX (2013) Study status and prospects of mine pressure bumping control technology in China. *Coal Sci Technol* 41(6):21–25 (in Chinese)
- Tang CA, Wang JM, Zhang JJ (2010) Preliminary engineering application of microseismic monitoring technique to rockburst prediction in tunneling of Jinping II project. *J Rock Mech Geotech Eng* 2(3):193–208
- Tang LZ, Zhang J, Li XB (2012) Research on response of mine microseismicity to mining rate based on quantitative seismology. *Int J Rock Mech Min Sci* 31(7):1343–1354
- Wang EY, He XQ, Wei JP, Nie BS, Song DZ (2011) Electromagnetic emission graded warning model and its applications against coal rock dynamic collapses. *Int J Rock Mech Min Sci* 48:556–564
- Wang GF, Gons SY, Li ZL, Dou LM, Cai W, Mao Y (2015) Evolution of stress concentration and energy release before rock bursts two case studies from Xingan coal mine, Hegang, China. *Rock Mech Rock Eng* 45:1–9
- Williams TJ, Wideman CJ, Scott DF (1992) Case history of a slip-type rock burst. *Pure appl Geophys* 139:627–637
- Xia YX, Kang LJ, Qi QX, Mao DB, Ren Y, Lan H, Pan JF (2010) Five indexes of microseismic and their application in rock burst forecast. *J China Coal Soc* 35(12):2011–2016 (in Chinese)
- Xie HP, Pariseau WG (1993) Fractal character and mechanism of rock bursts. *Rock Mech Min Sci* 30(4):343–350
- Xu NW, Tang CA, Li LC, Zhou Z, Sha C, Liang ZZ, Yang JY (2011) Microseismic monitoring and stability analysis of the left bank slope in Jinping first stage hydropower station in southwestern China. *Int J Rock Mech Min Sci* 48(6):950–963
- Yamada T, Mori JJ, Ide S, Abercrombie RE, Kawakata H, Nakatani M, Iio Y, Ogasawara H (2007) Stress drops and radiated seismic energies of microearthquakes in a South African gold mine. *J Geophys Res* 112:1–12
- Zhang MW, Shimada H, Sasaoka T, Matsui K, Dou LM (2013) Seismic energy distribution and hazard assessment in underground coal mines using statistical energy analysis. *Int J Rock Mech Min Sci* 64:192–200
- Zhang N, Zhang NC, Han CL, Qian DY, Xue F (2014) Borehole stress monitoring analysis on advanced abutment pressure induced by Longwall Mining. *Arab J Geosci* 7:457–463
- Zhu ST, Feng Y, Jiang FX (2015) Determination of abutment pressure in coal mines with extremely thick alluvium stratum: a typical kind of rockburst mines in China. *Rock Mech Rock Eng* 49(5):1943–1952